750

SANDIA REPORT SAND82-1055 • Unlimited Release • UC-70
Printed July 1982

# Uniaxial Compression Test Series on Tram Tuff

Ronald H. Price, Karol G. Nimick

Prepared by
Sandia National Laboratories
Albuquerque, New Mexico 87185 and Livermore, California 94550
for the United States Department of Energy
under Contract DE-AC04-76DP00789

SF2900Q(8-81)

Issued by Sandia National Laboratories, operated for the United States Department of Energy by Sandia Corporation.


Printed in the United States of America
Available from
National Technical Information Service
U.S. Department of Commerce
5285 Port Royal Road
Springfield, VA 22161

NTIS price codes
Printed copy: A03
Microfiche copy: A01

SAND82-1055
Unlimited Release

# Uniaxial Compression Test Series on Tram Tuff*

Ronald H. Price and Karol G. Nimick
Sandia National Laboratories
Albuquerque, New Mexico 87185

## ABSTRACT

Twenty-five uniaxial compression experiments were performed on samples of the Tram Member of the Crater Flat Tuff obtained from drill hole USW-G1 at Yucca Mountain on the Nevada Test Site. The water saturated samples were deformed at nominal strain rates ranging from $10^{-2}$ to $10^{-6}$ $sec^{-1}$, atmospheric pressure and room temperature. Resultant unconfined compressive strengths, axial strains to failure, Young's moduli and Poisson's ratios ranged from 14.5 to 69.2 MPa, .0029 to .0052, 5.17 to 22.5 GPa and .09 to .38, respectively.

* This work performed at Sandia National Laboratories supported by the U. S. Department of Energy under Contract Number DE-AC04-76-DP00789.

TABLE OF CONTENTS

## LIST OF SYMBOLS AND CONVENTIONS

| | |
|---|---|
| $\sigma_1$, $\sigma_2$, $\sigma_3$ | Principal stresses (force/original area); compressive stresses are positive |
| $\epsilon_1$, $\epsilon_2$, $\epsilon_3$ | Principal strains (change in length/original length); compressive strains are positive |
| $\sigma_{AX}$, $\epsilon_{AX}$ | Stress and strain parallel to cylinder axis (i.e., $\sigma_{AX} = \sigma_1$ and $\epsilon_{AX} = \epsilon_1$) |
| $\epsilon_{LAT}$ | Strain perpendicular to cylinder axis (i.e., lateral strain (= $\epsilon_2 = \epsilon_3$)) |
| $(\sigma_{AX})_u$ | Ultimate axial stress |
| $(\epsilon_{AX})_u$ | Axial strain corresponding to ultimate axial stress |
| E, $\nu$ | Elastic moduli (Young's modulus, Poisson's ratio) |
| F | Force |
| d | Displacement |
| T | Temperature |
| P | Pressure |
| t | Time |
| $\phi$ | Porosity |
| $\rho_g$ | Grain Density |

## INTRODUCTION

Yucca Mountain, near the southwest margin of the Nevada Test Site (NTS) in southern Nevada, is being evaluated as a potential site for underground storage of nuclear wastes. Yucca Mountain primarily consists of layered volcanic tuff (Lipman and McKay, 1965). At present, four stratigraphic units are being tested for physical, thermal and mechanical properties as part of the Nevada Nuclear Waste Storage Investigations (NNWSI) Project, administered by the Nevada Operations Office of the U. S. Department of Energy. The four units, in order of increasing stratigraphic position (decreasing depth and age), are as follows: 1. Tram Member of the Crater Flat Tuff, 2. Bullfrog Member of the Crater Flat Tuff, 3. The Tuffaceous beds of Calico Hills, and 4. Topopah Spring Member of the Paintbrush Tuff.

This report is the second in the series of four, presenting data from twenty-five mechanical tests conducted on samples of Tram Tuff. The test specimens were obtained from USW-G1 core at eleven different stratigraphic levels ranging in depth from 822.7 to 1066.3 m (2699.1 to 3498.4 ft). The test specimens were saturated and deformed at nominal strain rates of $10^{-2}$, $10^{-4}$, $10^{-5}$ and $10^{-6}$ $sec^{-1}$; atmospheric confining pressure; and room temperature.

As was noted in the Bullfrog Tuff data report (Price, et al., 1982), a detailed analysis of the mechanical data from all Yucca Mountain tuffs will be reported at the conclusion of the four test series.

## EXPERIMENTAL TECHNIQUES

### Test Apparatus and Techniques

The mechanical experiments were performed on a load frame having a maximum load capacity of 0.1 MN (22 kip). A constant displacement rate of the loading piston is achieved by servo-control of the hydraulic loading ram while monitoring an LVDT (linear variable displacement transformer) at the base of the loading column.

Throughout this test series, axial stresses were calculated by dividing the forces, measured on a standard load cell, by the original cross-sectional area of the sample. Axial strains were calculated by averaging the measured displacements on two diametrically opposed LVDT's mounted directly on the sample and dividing the average value of the original gage length. Lateral (transverse) displacements were measured across one sample diameter by a disk gage (as described by Schuler, 1978). Lateral strains were then obtained by dividing the displacements by the diameter of the test specimen. Volumetric strains were computed from axial and transverse strain data. Axial force, axial displacement, transverse displacement, ram displacement and time data were collected, reduced and plotted by a mini-computer, and then stored on floppy disks.

## Calibrations

The test system load cell is calibrated against a standard transducer once a year. The most recent load cell evaluation was performed March 24, 1981. The axial displacement LVDT's and transverse displacement gage were calibrated with a standard micrometer head prior to the test series. Calibration data for the load cell, LVDT's and gage are listed in Table I.

As a calibration test of the entire mechanical testing system, an aluminum sample of known mechanical properties was tested. The resultant data are listed and plotted in Table II and Figure 1, respectively.

## Sample Preparation

The samples were all right circular cylinders recored from drill hole USW-G1 core material. The experimental specimens were 2.53 cm (.998 in) in diameter and ranged in lengths from 5.088 to 5.105 cm (2.003 to 2.010 in).

The samples were stored in ground water from well J-13 (NTS) and, while submerged, subjected to a vacuum (≤ 2 Torr = 267 Pa) for 18 hours in order to be sure of sample saturation. Each sample was placed between steel end pieces and jacketed in polyolefin shrink tubing. The disk gage and two LVDT's were then mounted on the specimen, the sample assembly placed between the loading ram and the load cell and the mechanical experiment begun.

## EXPERIMENTAL RESULTS

### Test Conditions

The twenty-five mechanical experiments in this series were all unconfined compressive tests run at room temperature (i.e., approximately 23°C). Eighteen samples were obtained from ten depth intervals of USW-G1 core and tested at a nominal strain rate of $10^{-5}$ $sec^{-1}$. The remaining seven specimens, all from a depth of 976.2 m (3202.7 ft), were deformed at rates of $10^{-2}$, $10^{-4}$ and $10^{-6}$ $sec^{-1}$. This limited set of test conditions was chosen as a result of time constraints and a limited number of samples.

The test/sample identification used throughout this report consists of ten numbers and letters representing the drillhole (G1), sample depth (in feet), Sandia Laboratory (SL) and one letter (A, B, D, E, F, G, I, or J) identifying individual samples from the same depth.

### Test Data

Tabulated ultimate axial stress, axial strain to failure and elastic moduli values are given in Table III. The ranges of unconfined strengths, axial strains at failure, Young's moduli and Poisson's ratios are 14.5-69.2 MPa, .0029-.0052, 5.17-22.5 GPa and .09-.38, respectively. These large ranges in mechanical property data are not the result of random scatter, but to variations in the physical and petrologic characteristics of the tuffs. As stated earlier, formal data analysis will be presented in a later report.

The experimental axial stress-axial strain curves are presented in Figures 2, 3, 4 and 5. The general shapes of the stress-strain curves are very similar to those previously reported (Price, et al., 1982) from tests on Bullfrog Tuff, with an initial concave upward portion, a linear region, a slight concave downward portion and a sharp downward break. These curve characteristics reflect pore collapse and compaction, elastic deformation, material yield and macroscopic failure of the test specimen, respectively.

Considering the inherent scatter in all rock mechanics data, most of the curve sets presented in Figure 2 are very reproducible (see Figures 2A, B, C, E, G, I, J). Sample G12996.9SLD (Figure 2D) may have a large, soft grain or void (although none were externally observed) which resulted in a lower strength value than the other sample from the same depth (G12996.9SLB). Only one sample was deformed from each of two depths (see Figures 2F and H); consequently, the results are assumed to be representative (i.e., not anomalous) of intact tuff from each of those stratigraphic levels.

The experimental curves in Figures 3, 4 and 5 exhibit more general scatter. This result is probably due to a great deal of inhomogeneity in the physical characteristics of the tuff from 976.2 m depth. For example, several of the test specimens (G13202.7 SLA, SLD and SLE) contained large voids (0.5 to 1.0 cm) on the external surface.

The axial strain-time, axial stress-axial strain and lateral strain-axial strain data for these experiments is nearly identical to the data presented in the Bullfrog Tuff report (Price, et al., 1982). For curve trends, this earlier reference can be used.

## SUMMARY

Twenty-five samples of Tram Tuff were saturated and deformed in compression at nominal strain rates of $10^{-2}$, $10^{-4}$, $10^{-5}$ and $10^{-6}$ $sec^{-1}$, atmospheric pressure and room temperature. All of the samples exhibited an axial stress-axial strain behavior resulting in macroscopic brittle failure. The resultant unconfined compressive strengths, axial strains to failure, Young's moduli and Poisson's ratio ranged from 14.5 to 69.2 MPa, .0029 to .0052, 5.17 to 22.5 GPa and .09 to .38, respectively.

## REFERENCES

Lipman, P. W. and E. J. McKay (1965), Geologic Map of the Topopah Spring SW Quadrange, Nye County, Nevada, United States Geological Survey, USGS Map GQ-439.

Price, R. H., A. K. Jones and K. G. Nimick (1982), Uniaxial Compression Test Series on Bullfrog Tuff, Sandia Report, SAND82-0481, Sandia National Laboratories, Albuquerque, New Mexico, 40 p.

Schuler, K. W. (1978), Lateral-Deformation Gage for Rock Mechanics Testing, Experimental Mechanics, V. 18, No. 12, p. 477-480.

Table I. Load Cell, LVDT's and Disk Gage Calibration Data

Load Cell

| $F_A$ [a] | $F_{LC}$ [b] | $E$ [c] |
|---|---|---|
| 4.0 | 3.998 | -.05 |
| 8.0 | 7.992 | -.10 |
| 12.0 | 11.996 | -.03 |
| 16.0 | 16.000 | 0.0 |
| 20.0 | 20.016 | .08 |

LVDT's

| $d_A$ [d] | $d_L$ [e] | $E$ [c] |
|---|---|---|
| 2.0 | 2.018 | .90 |
| 5.0 | 5.046 | .92 |
| 8.0 | 8.042 | .53 |
| 10.0 | 10.048 | .48 |
| 12.0 | 12.052 | .43 |
| 15.0 | 15.034 | .23 |
| 18.0 | 18.014 | .08 |
| 20.0 | 19.992 | -.04 |

Disk Gage

| $d_A$ [d] | $d_G$ [e] | $E$ [c] |
|---|---|---|
| 2.0 | 2.008 | .40 |
| 4.0 | 4.014 | .35 |
| 6.0 | 6.040 | .67 |
| 8.0 | 8.048 | .60 |
| 10.0 | 10.060 | .60 |
| 12.0 | 12.032 | .27 |
| 14.0 | 14.020 | .14 |
| 16.0 | 16.010 | .06 |
| 18.0 | 18.006 | .03 |
| 20.0 | 20.000 | 0.0 |

[a] Force (kilopounds) measured by the standard load cell.
[b] Force (kilopounds) measured by the system's load cell.
[c] Error (percent) in system measurement.
[d] Displacement (milliinches) measured by the standard micrometer.
[e] Displacement (milliinches) measured by the disk gage or LVDT set.

Table II. Aluminum Sample Calibration Data

| $\sigma_{AX}$ (MPa) | $\epsilon_{AX}$ (Millistrain) | $-\epsilon_{LAT}$ (Millistrain) |
|---|---|---|
| 0.00 | 0.00 | 0.00 |
| 3.27 | .0409 | .0128 |
| 7.26 | .107 | .0322 |
| 9.57 | .141 | .0398 |
| 13.0 | .191 | .0628 |
| 16.2 | .233 | .0689 |
| 19.4 | .282 | .0919 |
| 22.7 | .315 | .110 |
| 26.0 | .372 | .121 |
| 29.4 | .411 | .139 |
| 32.8 | .454 | .165 |
| 36.1 | .503 | .168 |
| 39.1 | .541 | .173 |
| 42.4 | .579 | .192 |
| 45.6 | .631 | .212 |
| 48.6 | .665 | .236 |
| 52.2 | .719 | .245 |
| 55.5 | .764 | .252 |
| 58.7 | .812 | .269 |

Table III. Experimental Data

| Sample ID | Depth m | Depth (ft) | $\dot{\epsilon}$ ($sec^{-1}$) | $(\sigma_{AX})_u$ (MPa) | $(\epsilon_{AX})_u$ (%) | $E^a$ (GPa) | $\nu^a$ | $\phi^b$ (%) | $\rho_g^b$ (g/cm$^3$) |
|---|---|---|---|---|---|---|---|---|---|
| G12699.1 SLB | 822.7 | (2699.1) | $10^{-5}$ | 60.1 | .46 | 14.5 | .16 | 32.9 | 2.52 |
| G12699.1 SLD | 822.7 | (2699.1) | $10^{-5}$ | 53.6 | .51 | 13.3 | .18 | 32.9 | 2.52 |
| G12810.0 SLB | 856.5 | (2810.0) | $10^{-5}$ | 42.0 | .36 | 15.2 | .38 | 23.4 | 2.61 |
| G12810.0 SLD | 856.5 | (2810.0) | $10^{-5}$ | 46.0 | .43 | 14.2 | .31 | 23.4 | 2.61 |
| G12897.0 SLB | 883.0 | (2897.0) | $10^{-5}$ | 68.1 | .43 | 21.3 | .27 | 21.4 | 2.62 |
| G12897.0 SLD | 883.0 | (2897.0) | $10^{-5}$ | 69.2 | .46 | 19.9 | .24 | 21.4 | 2.62 |
| G12996.9 SLB | 913.4 | (2996.9) | $10^{-5}$ | 67.6 | .37 | 22.5 | .23 | 20.5 | 2.59 |
| G12996.9 SLD | 913.4 | (2996.9) | $10^{-5}$ | 40.9 | .29 | 18.9 | --- | 20.5 | 2.59 |
| G13030.9 SLB | 923.8 | (3030.9) | $10^{-5}$ | 33.1 | .37 | 13.4 | --- | 26.4 | 2.58 |
| G13030.9 SLD | 923.8 | (3030.9) | $10^{-5}$ | 28.6 | .46 | 10.5 | .28 | 26.4 | 2.58 |
| G13102.3 SLD | 945.6 | (3102.3) | $10^{-5}$ | 20.2 | .42 | 5.80 | .20 | 25.5 | 2.56 |
| G13200.2 SLB | 975.4 | (3200.2) | $10^{-5}$ | 33.0 | .47 | 8.60 | .17 | 17.6 | 2.61 |
| G13200.2 SLD | 975.4 | (3200.2) | $10^{-5}$ | 25.8 | .48 | 7.36 | --- | 17.6 | 2.61 |
| G13202.7 SLA | 976.2 | (3202.7) | $10^{-2}$ | 31.1 | .52 | 6.63 | --- | 17.6 | 2.61 |
| G13202.7 SLG | 976.2 | (3202.7) | $10^{-2}$ | 24.4 | .50 | 5.17 | --- | 17.6 | 2.61 |
| G13202.7 SLD | 976.2 | (3202.7) | $10^{-4}$ | 25.3 | .50 | 6.42 | --- | 17.6 | 2.61 |
| G13202.7 SLE | 976.2 | (3202.7) | $10^{-4}$ | 22.1 | .32 | 8.76 | --- | 17.6 | 2.61 |
| G13202.7 SLF | 976.2 | (3202.7) | $10^{-4}$ | 32.6 | .44 | 8.97 | .089 | 17.6 | 2.61 |
| G13202.7 SLI | 976.2 | (3202.7) | $10^{-6}$ | 14.5 | .31 | 7.04 | .30 | 17.6 | 2.61 |
| G13202.7 SLJ | 976.2 | (3202.7) | $10^{-6}$ | 26.5 | .50 | 8.26 | .14 | 17.6 | 2.61 |
| G13308.0 SLB | 1008.3 | (3308.0) | $10^{-5}$ | 25.6 | .33 | 8.47 | .26 | 22.0 | 2.64 |
| G13405.2 SLB | 1037.9 | (3405.2) | $10^{-5}$ | 30.0 | .35 | 8.85 | .18 | 18.4 | 2.66 |
| G13405.2 SLD | 1037.9 | (3405.2) | $10^{-5}$ | 37.3 | .34 | 12.4 | .31 | 18.4 | 2.66 |
| G13498.4 SLB | 1066.3 | (3498.4) | $10^{-5}$ | 17.8 | .35 | 5.56 | .31 | 19.4 | 2.69 |
| G13498.4 SLD | 1066.3 | (3498.4) | $10^{-5}$ | 17.4 | .31 | 5.47 | --- | 19.4 | 2.69 |

[a] All E and $\nu$ values were calculated at .5 $(\sigma_{AX})_u$.

[b] Bulk property data from A. R. Lappin (personal communication).

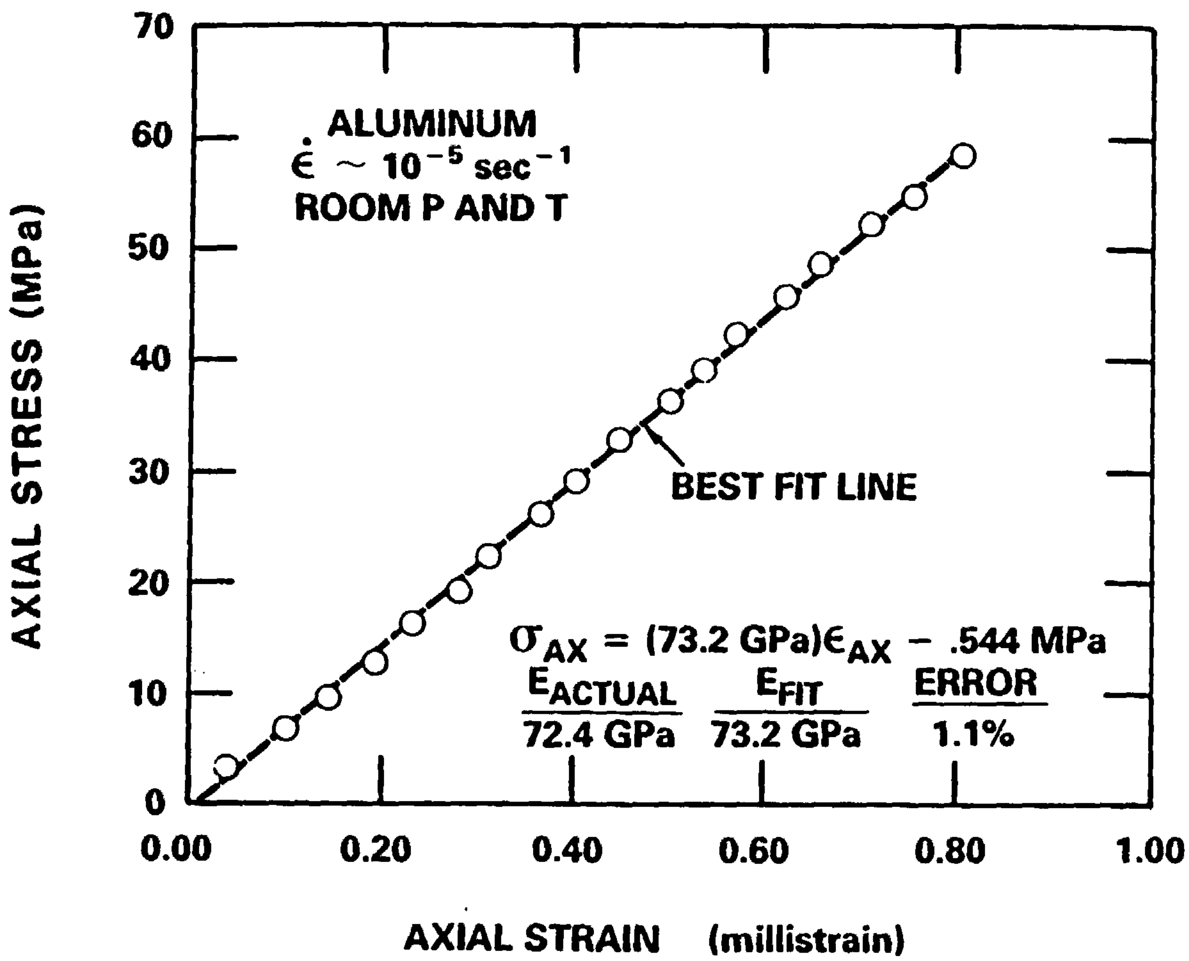


Figure 1A: Plot of axial stress-axial strain data with linear fit for system calibration with an aluminum sample.

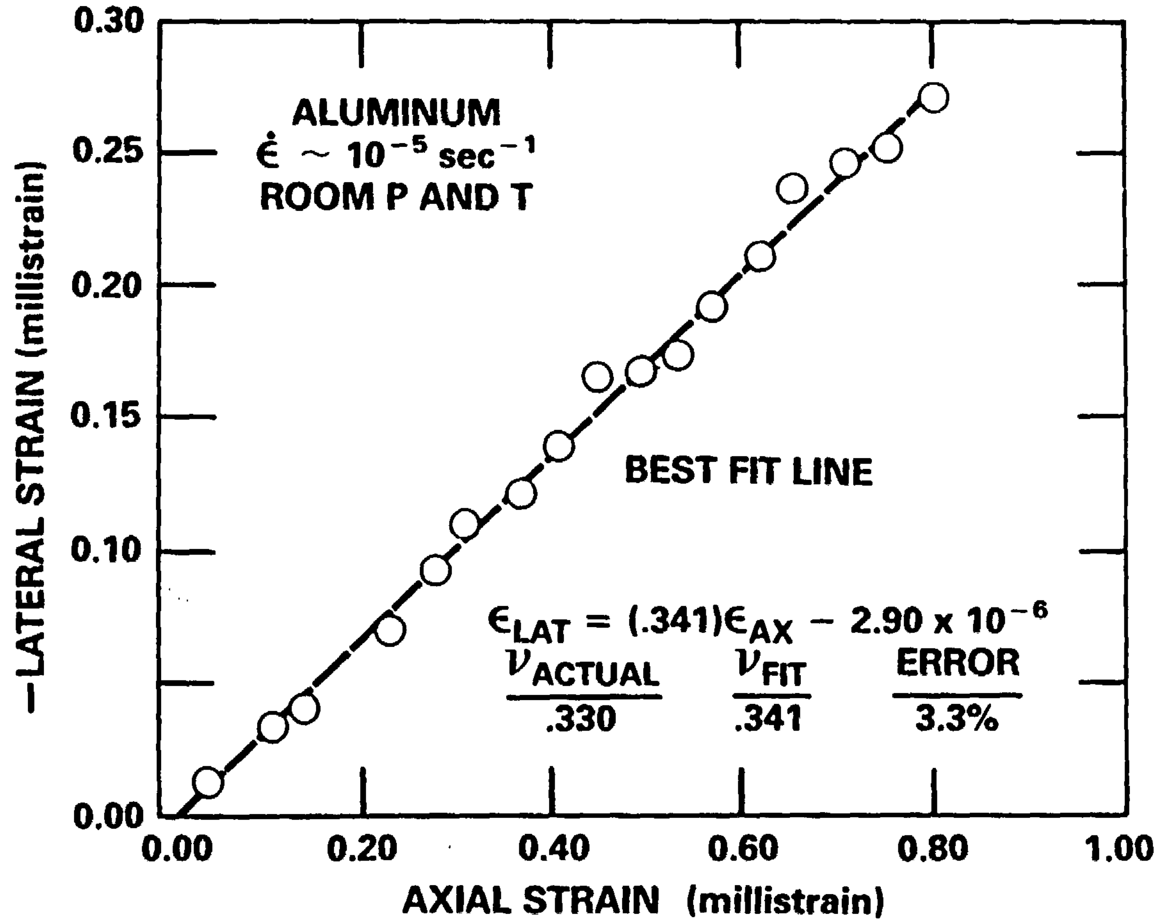


Figure 1B: Plot of lateral strain-axial strain data with linear fit for system calibration with an aluminum sample.

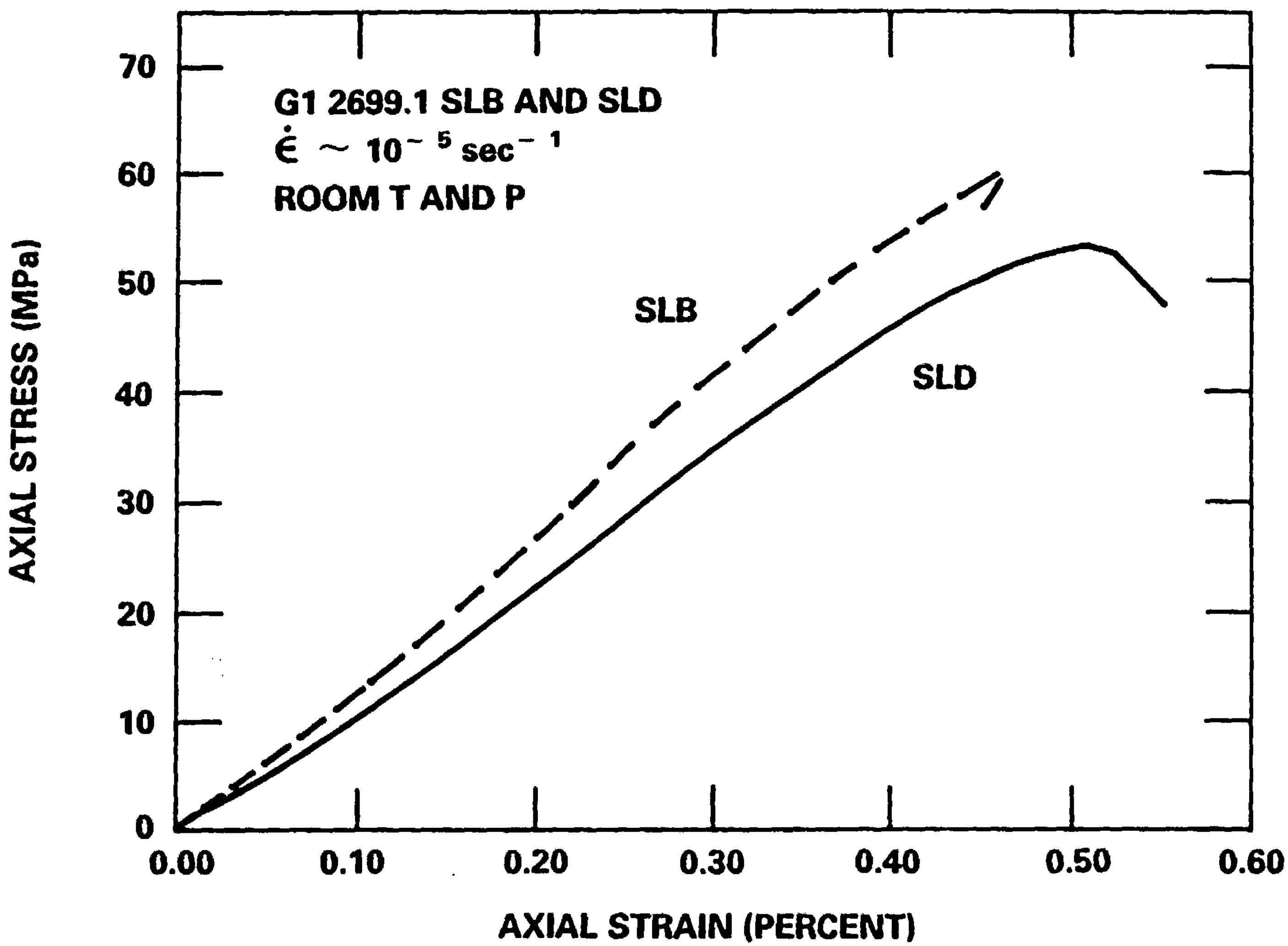


Figure 2A: Axial stress-axial strain curves for saturated samples G12699.1 SLB and SLD deformed in compression at a nominal strain rate of $10^{-5}$ $sec^{-1}$, atmospheric pressure and room temperature.

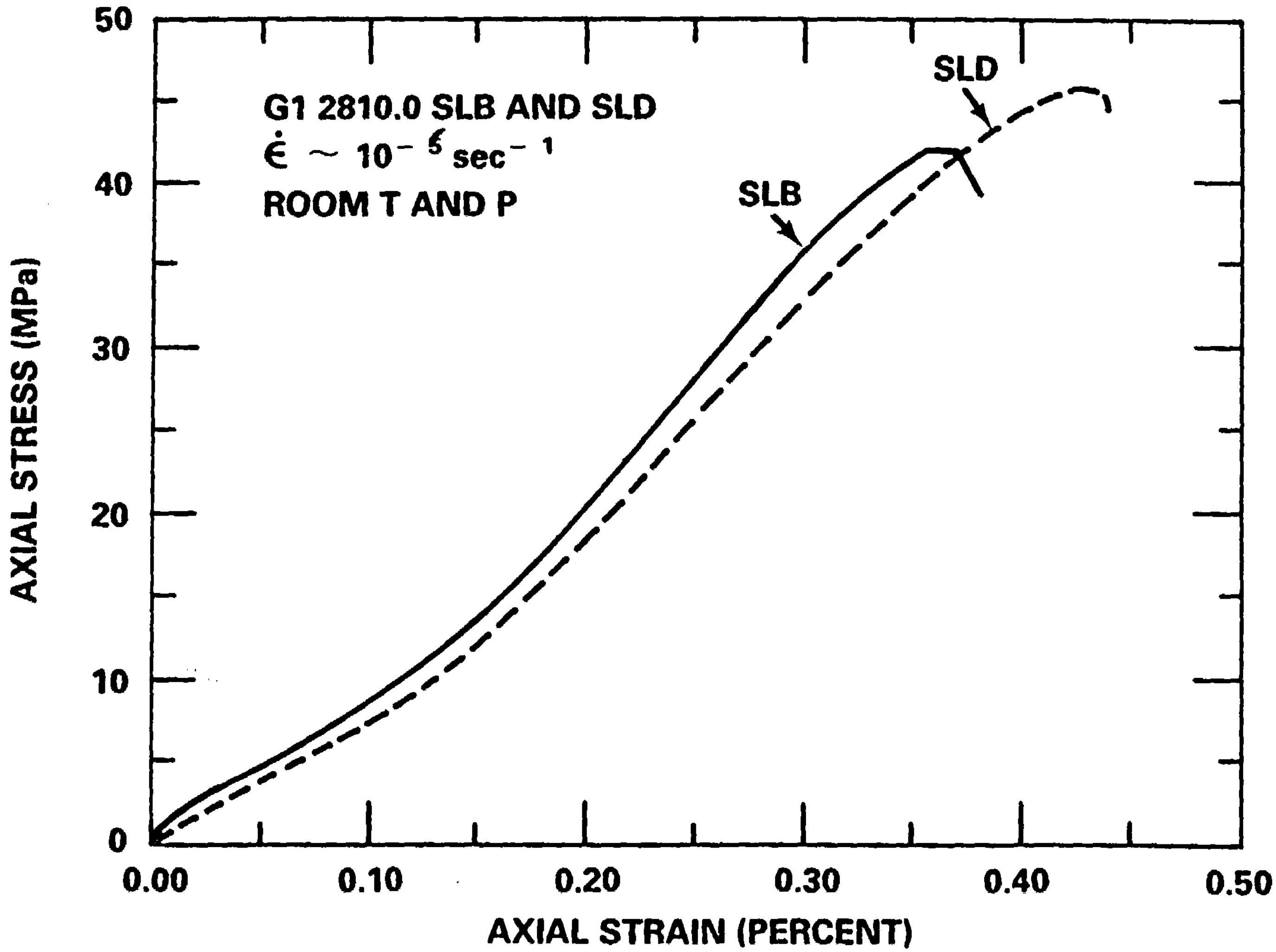


Figure 2B: Axial stress-axial strain curves for saturated samples G12810.0 SLB and SLD deformed in compression at a nominal strain rate of $10^{-5}$ $sec^{-1}$, atmospheric pressure and room temperature.

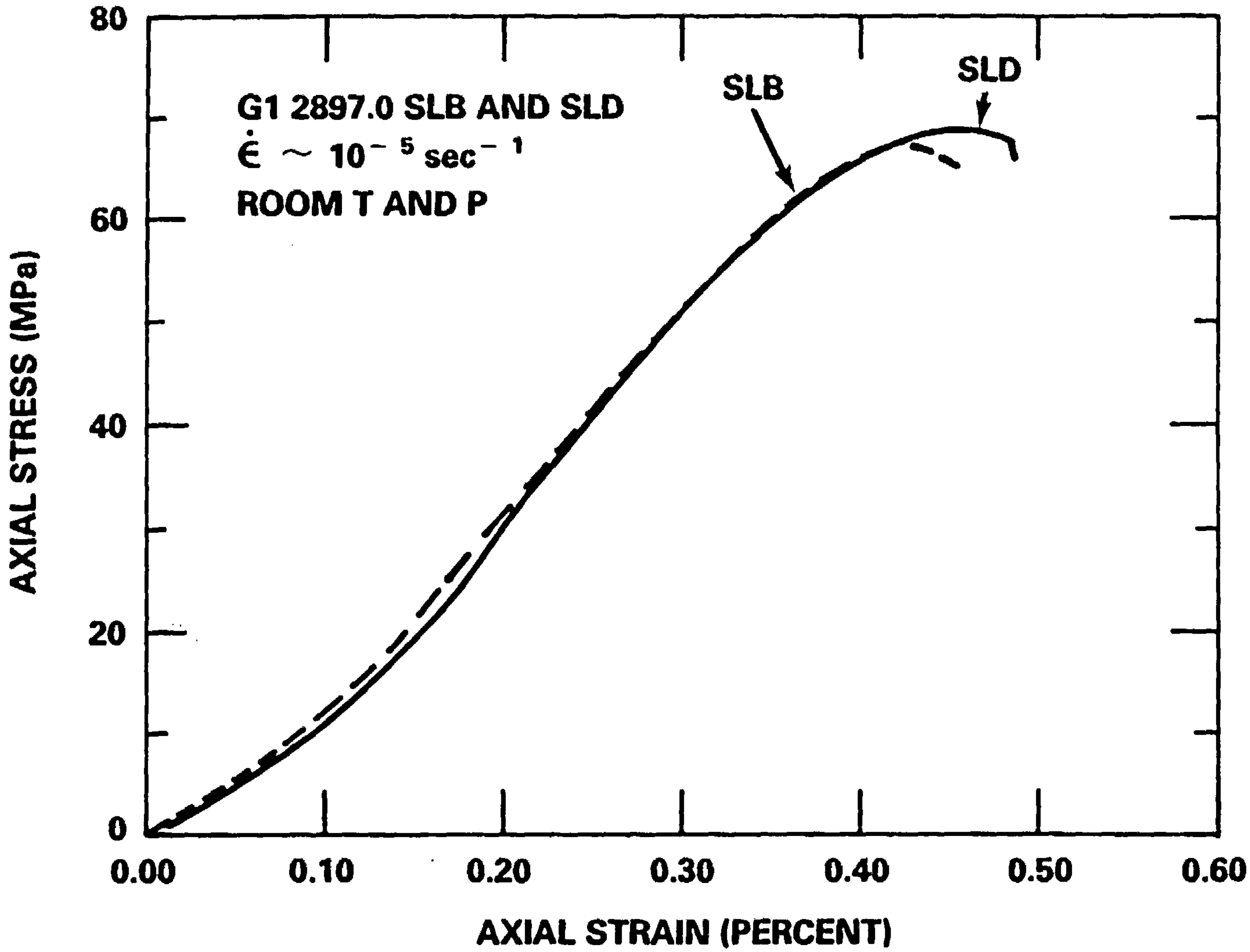


Figure 2C: Axial stress-axial strain curves for saturated samples G12897.0 SLB and SLD deformed in compression at a nominal strain rate of $10^{-5}$ sec$^{-1}$, atmospheric pressure and room temperature.

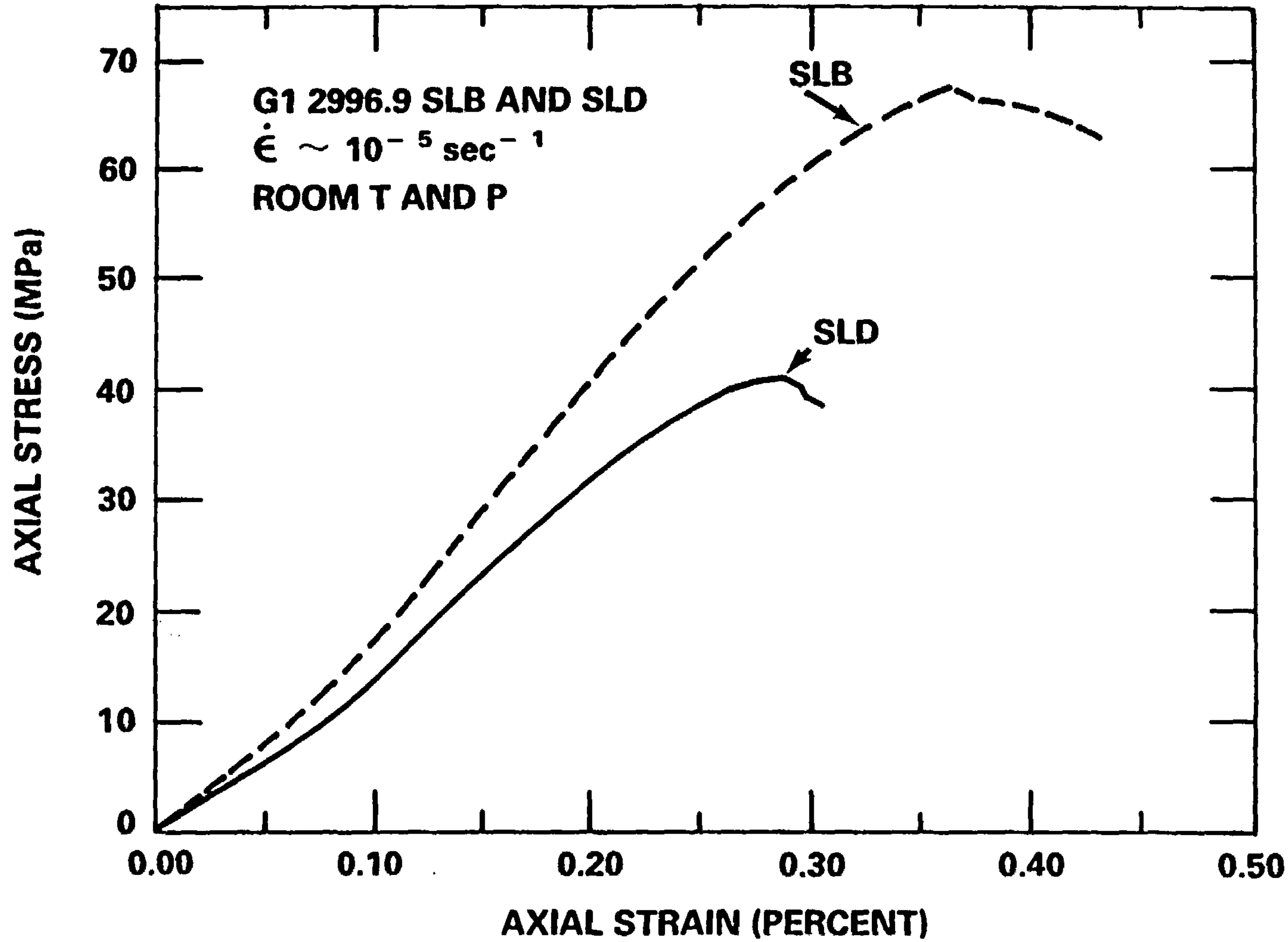


Figure 2D: Axial stress-axial strain curves for saturated samples G12996.9 SLB and SLD deformed in compression at a nominal strain rate of $10^{-5}$ $sec^{-1}$, atmospheric pressure and room temperature.

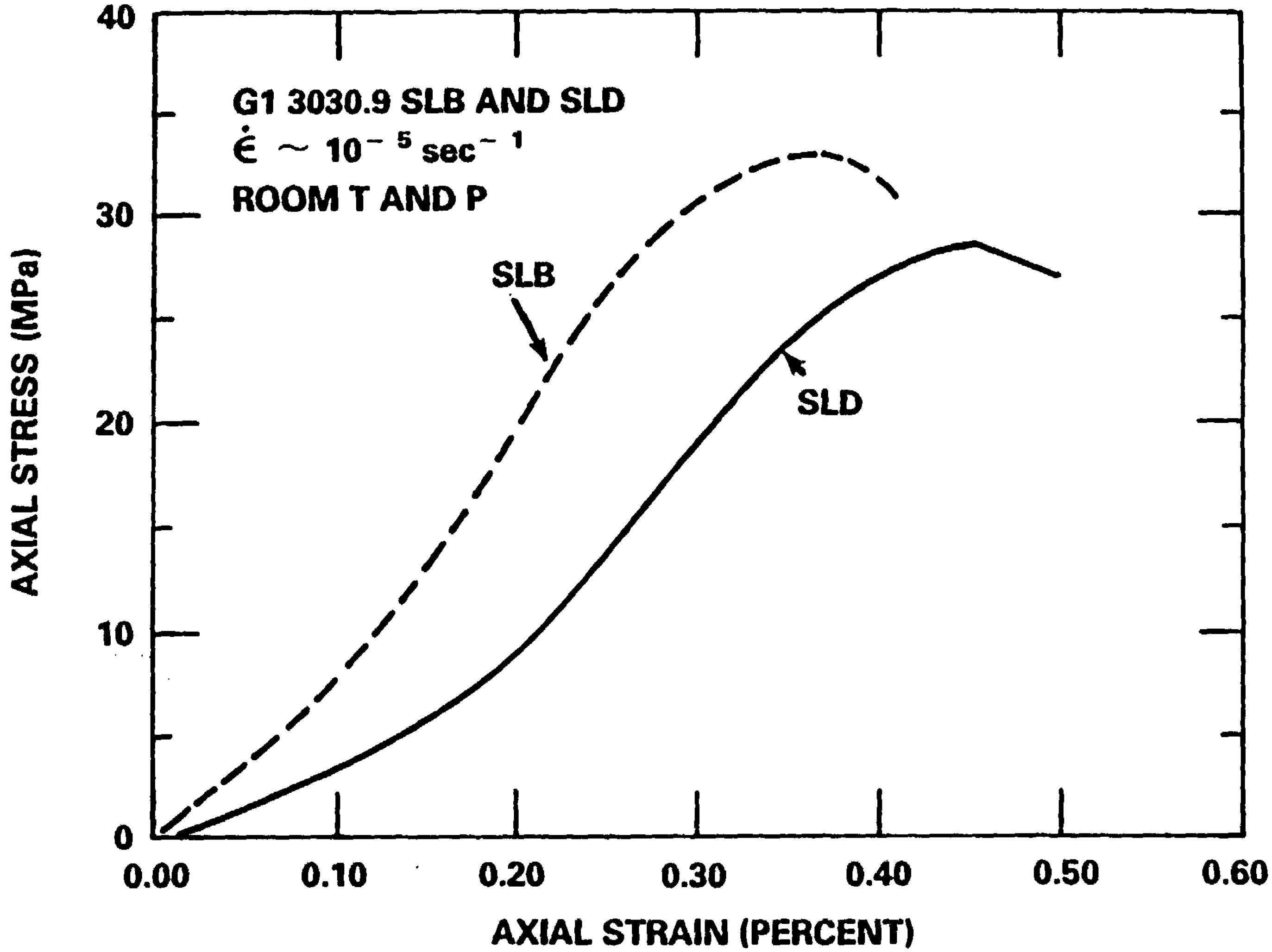


Figure 2E: Axial stress-axial strain curves for saturated samples G13030.9 SLB and SLD deformed in compression at a nominal strain rate of $10^{-5}$ sec$^{-1}$, atmospheric pressure and room temperature.

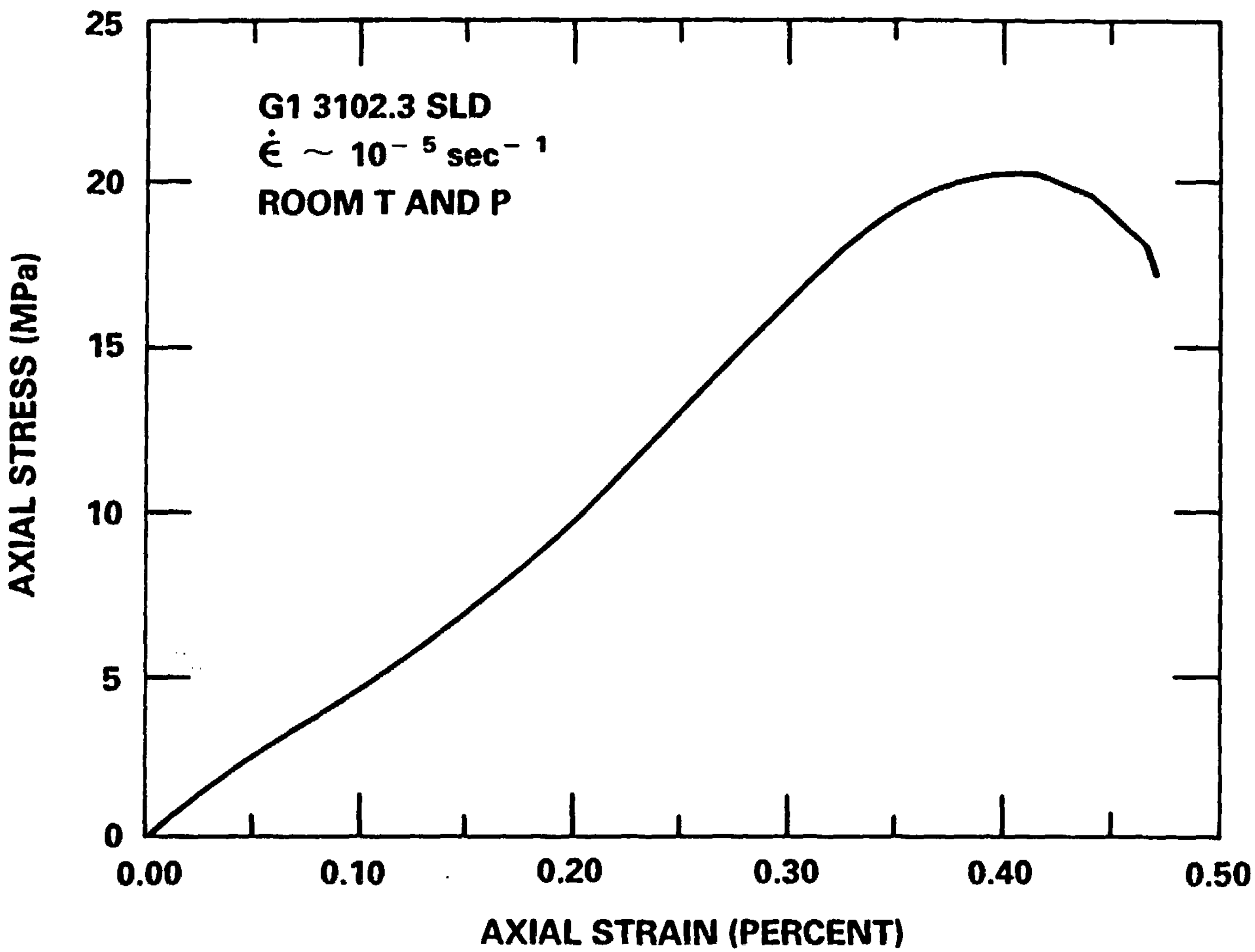


Figure 2F: Axial stress-strain curve for saturated sample G13102.3 SLD deformed in compression at a nominal strain rate of $10^{-5}$ sec$^{-1}$, atmospheric pressure and room temperature.

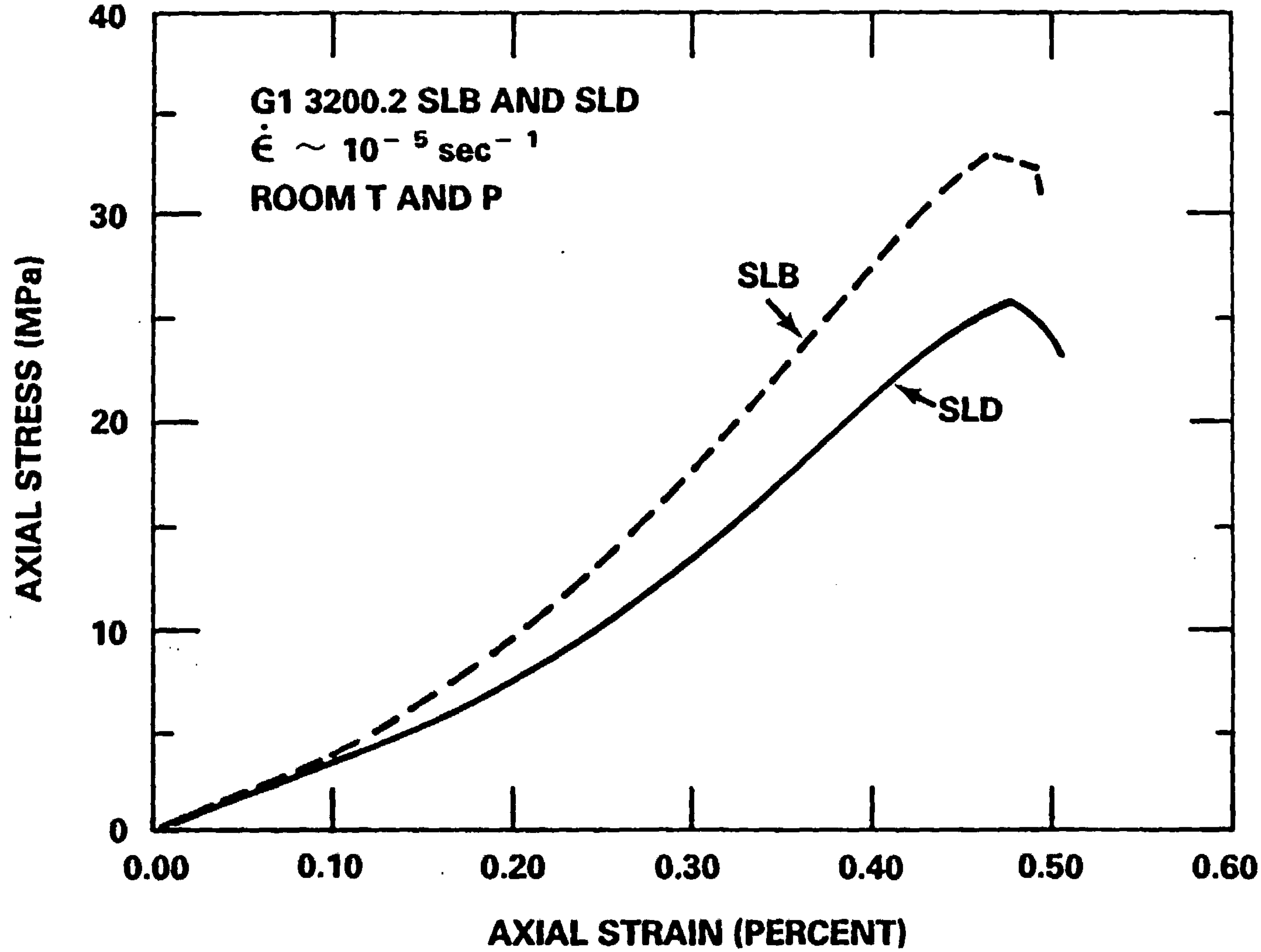


Figure 2G: Axial stress-axial strain curves for saturated samples G13200.2 SLB and SLD deformed in compression at a nominal strain rate of $10^{-5}$ sec$^{-1}$, atmospheric pressure and room temperature.

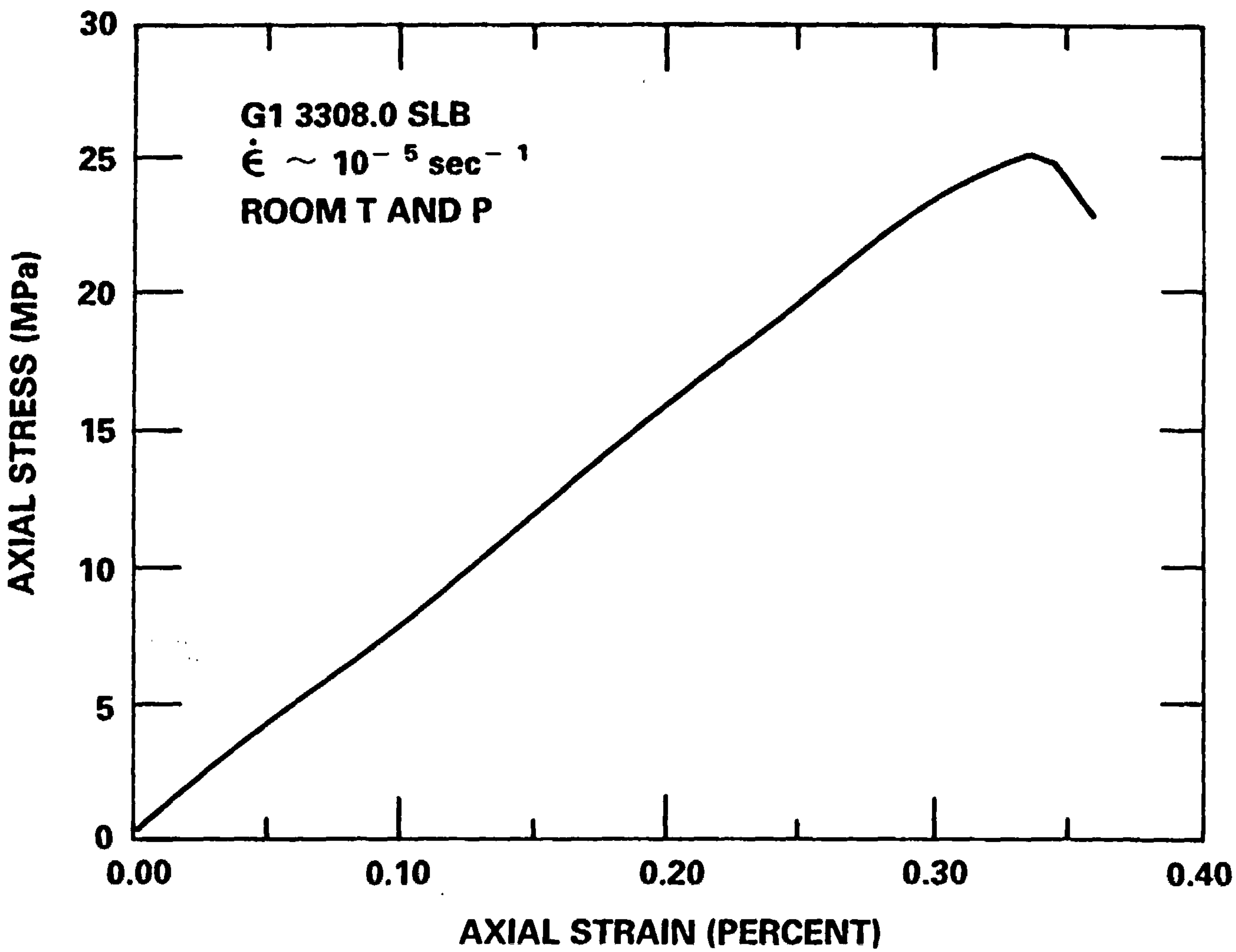


Figure 2H: Axial stress-axial strain curve for saturated sample G13308.0 SLB deformed in compression at a nominal strain rate of $10^{-5}$ $\mathrm{sec}^{-1}$, atmospheric pressure and room temperature.

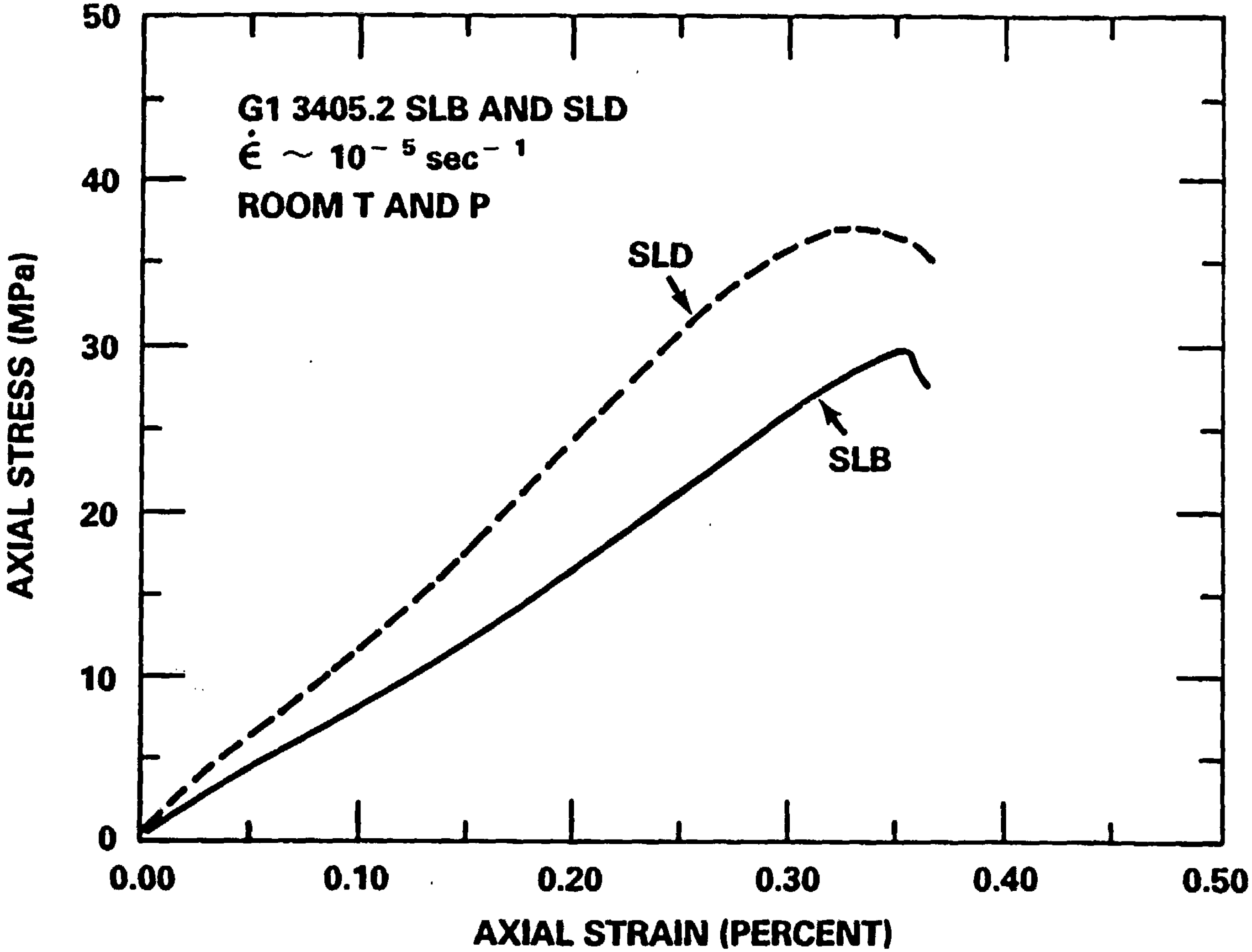


Figure 21: Axial stress-axial strain curves for saturated samples G13405.2 SLB and SLD deformed in compression at a nominal strain rate of $10^{-5}$ $sec^{-1}$, atmospheric pressure and room temperature.

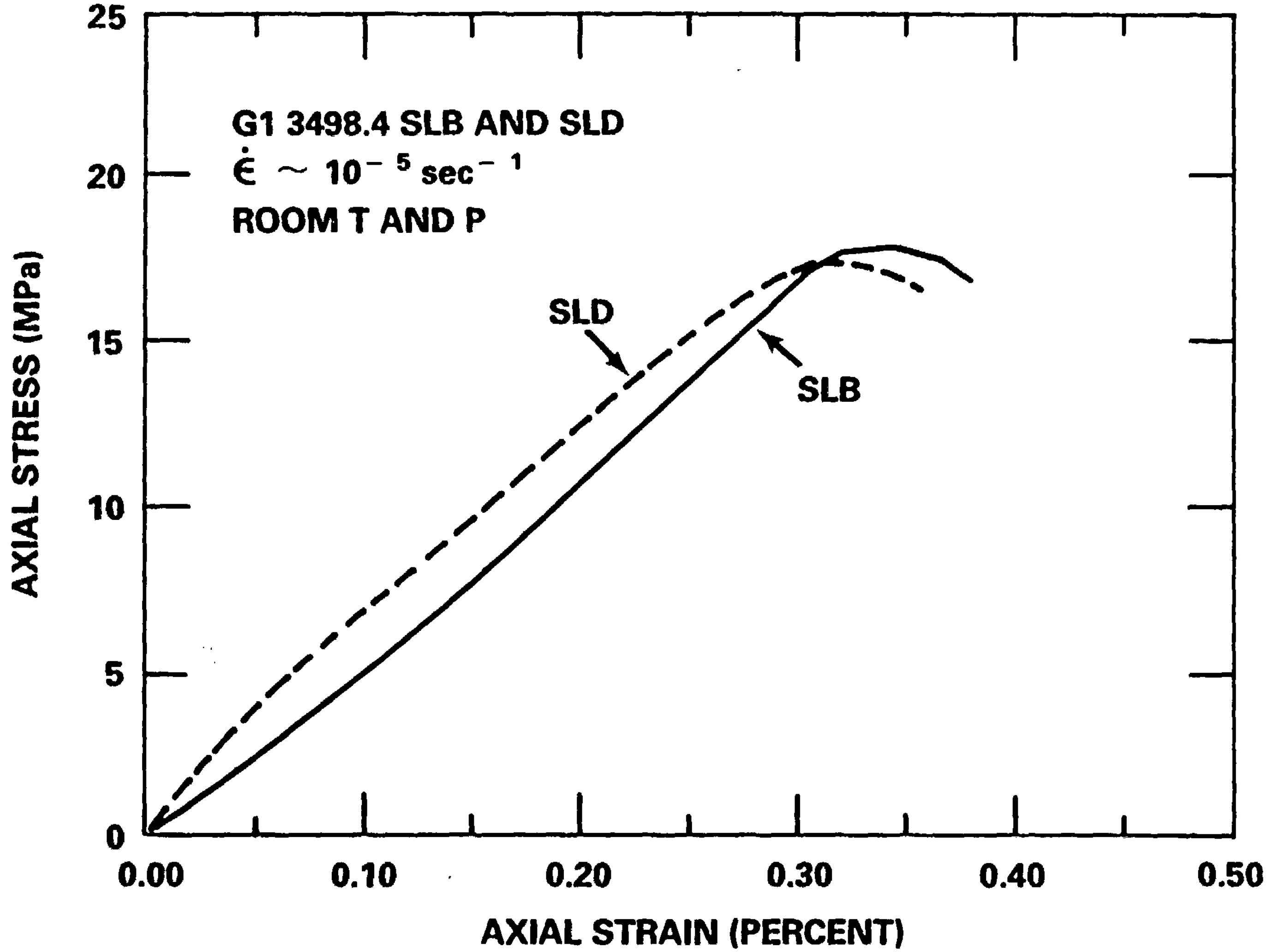


Figure 2J: Axial stress-axial strain curves for saturated samples G13498.4 SLB and SLD deformed in compression at a nominal strain rate of $10^{-5}$ sec$^{-1}$, atmospheric pressure and room temperature.

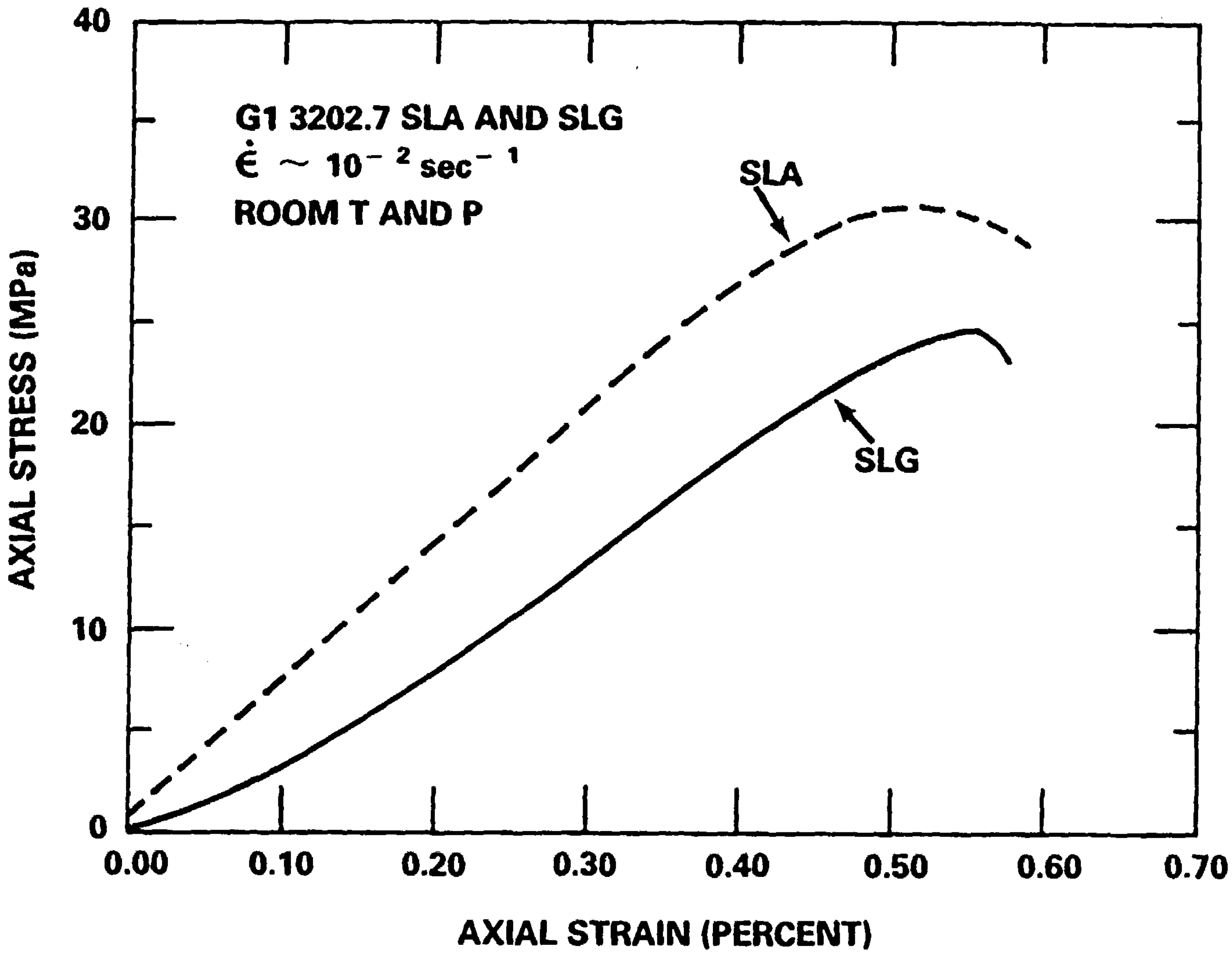


Figure 3: Axial stress-axial strain curves for saturated samples G13202.7 SLA and SLG deformed in compression at a nominal strain rate of $10^{-2}$ $sec^{-1}$, atmospheric pressure and room temperature.

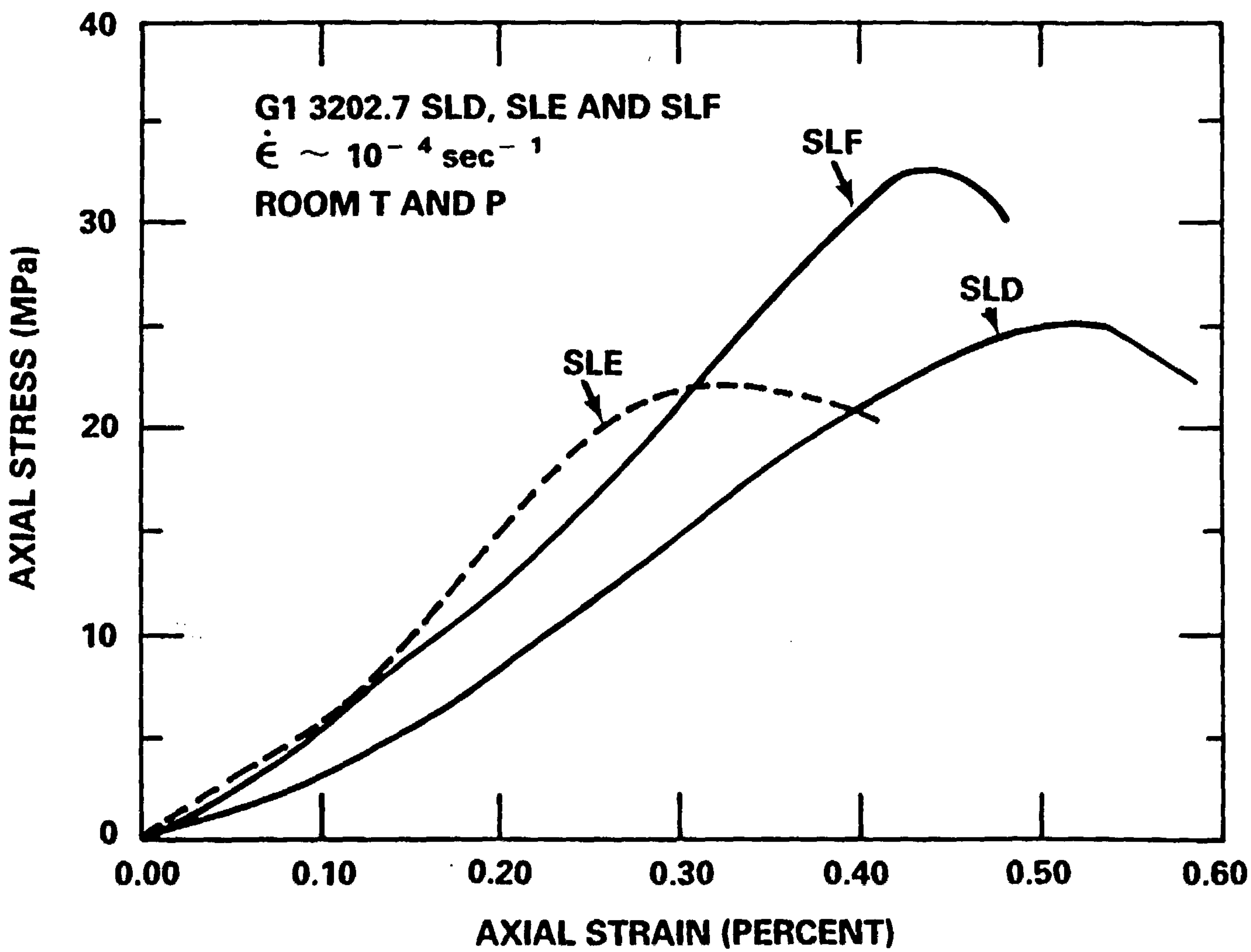


Figure 4: Axial stress-axial strain curves for saturated samples G13202.7 SLD, SLD and SLF deformed in compression at a nominal strain rate of $10^{-4}$ $sec^{-1}$, atmospheric pressure and room temperature.

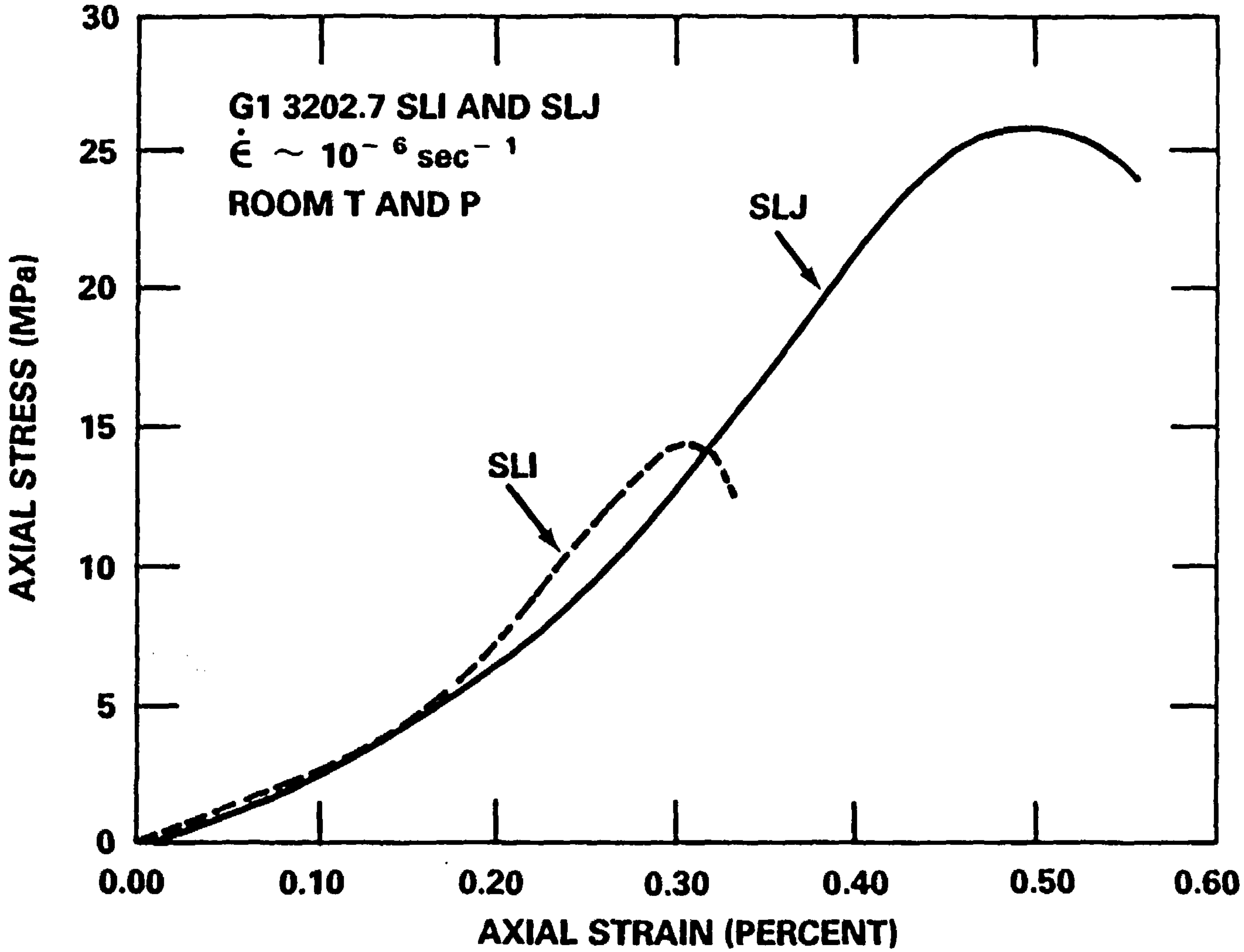


Figure 5: Axial stress-axial strain curves for saturated samples G13202.7 SLI and SLJ deformed in compression at a nominal strain rate of $10^{-6}$ $sec^{-1}$, atmospheric pressure and room temperature.

Distribution:
Unlimited Release

W. Ballard, Director
Office of Waste Isolation
U. S. Department of Energy
Room B-207
Germantown, MD 20767

R. Stein, Acting Team Leader
Technology Team
U. S. Department of Energy
Room B-220
Germantown, MD 20767

J. O. Neff, Program Manager
National Waste Terminal
Storage Program Office
U. S. Department of Energy
505 King Avenue
Columbus, OH 43201

L. D. Ramspott
Technical Project Officer
Lawrence Livermore National
Laboratory
University of California
P. O. Box 808
Mail Stop L-204
Livermore, CA 94550

B. R. Erdal
Technical Project Officer
Los Alamos National Laboratory
University of California
P. O. Box 1663
Mail Stop 514
Los Alamos, NM 87545

A. R. Hakl, Site Manager
Westinghouse - AESD
P. O. Box 708
Mail Stop 703
Mercury, NV 39023

G. L. Dixon
Technical Project Officer
U. S. Geological Survey
P. O. Box 25046
Mail Stop 954
Federal Center
Denver, CO 80301

W. E. Wilson
U. S. Geological Survey
P. O. Box 25045
Mail Stop 954
Denver, CO 80301

W. S. Twenhofel
820 Estes Street
Lakewood, CO 80226

C. R. Cooley, Deputy Director
Office of Waste Isolation
U. S. Department of Energy
Room B-214
Germantown, MD 20767

R. G. Goranson
U. S. Department of Energy
Richland Operations Office
P. O. Box 550
Richland, WA 99352

R. Deju
Rockwell International Atomics
International Division
Rockwell Hanford Operations
Richland, WA 99352

D. L. Vieth, Director (3)
Waste Management Project Office
U. S. Department of Energy
P. O. Box 14100
Las Vegas, NV 89114

D. F. Miller, Director
Office of Public Affairs
U. S. Department of Energy
P. O. Box 14100
Las Vegas, NV 89114

R. H. Marks
U. S. Department of Energy
CP-1, M/S 210
P. O. Box 14100
Las Vegas, NV 89114

B. W. Church, Director
Health Physics Division
U. S. Department of Energy
P. O. Box 14100
Las Vegas, NV 89114

R. R. Loux (7)
U. S. Department of Energy
P. O. Box 14100
Las Vegas, NV 89114

A. E. Gurrola
Holmes & Narver, Inc.
P. O. Box 14340
Las Vegas, NV 89114

K. Street, Jr.
Lawrence Livermore National
Laboratory
University of California
Mail Stop L-209
P. O. Box 808
Livermore, CA 94550

D. C. Hoffman
Los Alamos National Laboratory
Mail Stop 760
P. O. Box 1663
Los Alamos, NM 87545

N. E. Carter
Battelle
Office of Nuclear Waste Isolation
505 King Avenue
Columbus, OH 43201

W. A. Carbiener
Battelle
Office of NWTS Integration
505 King Avenue
Columbus, OH 43201

S. Goldsmith
Battelle
Office of Nuclear Waste Isolation
505 King Avenue
Columbus, OH 43201

ONWI Library (5)
Battelle
Office of Nuclear Waste Isolation
505 King Avenue
Columbus, OH 43201

R. M. Hill
State Planning Coordinator
Governor's Office of Planning
Coordination
State of Nevada
Capitol Complex
Carson City, NV 89023

N. A. Clark
Department of Energy
State of Nevada
Capitol Complex
Carson City, NV 89710

J. P. Colton
International Atomic Energy Agency
Division of Nuclear Power &
Reactors
Karnter Ring 11
P. O. Box 590, A-1011
Vienna, Austria

H. D. Cummingham
Reynolds Electrical and
Engineering Co., Inc.
Mail Stop 555
P. O. Box 14400
Las Vegas, NV 89114

J. A. Cross
Fenix & Scisson, Inc.
P. O. Box 15408
Las Vegas, NV 89114

A. M. Friedman
Argonne National Laboratories
9700 S. Cass Avenue
Argonne, IL 60439

A. J. Rothman (2)
Lawrence Livermore National
Laboratory
University of California
P. O. Box 808
Mail Stop L-204
Livermore, CA 94550

David K. Parrish
RE/SPEC, Inc.
P. O. Box 725
Rapid City, SD 57701

John W. Handin
Center for Tectonophysics
Texas A&M University
College Station, TX 77843

1112 A. J. Chabai
1417 F. W. Muller
3151 L. J. Erickson (5)
3151 W. L. Garner (3)
3154-3 C. Dalin (25)
For: DOE/TIC (Unlimited Release)
4760 R. W. Lynch
4761 L. W. Scully
4762 L. D. Tyler
4763 J. R. Tillerson
4763 A. R. Lappin
4764 R. C. Lincoln
4764 A. E. Stephenson
5500
5510 D. B. Hayes
5511 J. W. Nunziato
5511 W. D. Sundberg
5511 R. R. Eaton
5520 T. B. Lane
5521 R. D. Krieg
5521 R. K. Thomas
5524 L. W. Davison
5530 W. Herrmann
5531 B. J. Thorne
5531 M. L. Blanford
5532 B. M. Butcher
5532 L. S. Costin
5532 D. J. Holcomb
5532 K. G. Nimick
5532 W. A. Olsson
5532 R. H. Price (15)
5532 L. W. Teufel
5534 J. R. Asay
5541 W. C. Luth
8214 M. A. Pound